

# Temporal transformation of multiunit activity improves identification of single motor units

Gerwin Schalk<sup>a,\*</sup>, Jonathan S. Carp<sup>a,b</sup>, Jonathan R. Wolpaw<sup>a,b</sup>

<sup>a</sup> Wadsworth Center, New York State Department of Health, P.O. Box 509, Empire State Plaza, Albany, NY 12201-0509, USA

<sup>b</sup> School of Public Health, State University of New York, Albany, NY 12222, USA

Received 2 March 2001; received in revised form 26 November 2001; accepted 26 November 2001

## Abstract

This report describes a temporally based method for identifying repetitive firing of motor units. This approach is ideally suited to spike trains with negative serially correlated inter-spike intervals (ISIs). It can also be applied to spike trains in which ISIs exhibit little serial correlation if their coefficient of variation (COV) is sufficiently low. Using a novel application of the Hough transform, this method (i.e. the modified Hough transform (MHT)) maps motor unit action potential (MUAP) firing times into a feature space with ISI and offset (defined as the latency from an arbitrary starting time to the first MUAP in the train) as dimensions. Each MUAP firing time corresponds to a pattern in the feature space that represents all possible MUAP trains with a firing at that time. Trains with stable ISIs produce clusters in the feature space, whereas randomly firing trains do not. The MHT provides a direct estimate of mean firing rate and its variability for the entire data segment, even if several individual MUAPs are obscured by firings from other motor units. Addition of this method to a shape-based classification approach markedly improved rejection of false positives using simulated data and identified spike trains in whole muscle electromyographic recordings from rats. The relative independence of the MHT from the need to correctly classify individual firings permits a global description of stable repetitive firing behavior that is complementary to shape-based approaches to MUAP classification. © 2002 Elsevier Science B.V. All rights reserved.

*Keywords:* Motor unit action potential; Spike train; Hough transform; Temporal firing pattern; Decomposition; Spike sorting

## 1. Introduction

The pattern of discharge of motor unit action potentials (MUAPs) provides insight into the firing behavior of motoneurons. Potential information increases with increasing numbers of MUAPs in the recorded electromyographic activity (EMG) in parallel with increasing difficulty in their separation and identification. Resolution of multi-motor unit EMG into its constituent MUAPs usually is achieved by identifying times of likely discharges (i.e. MUAP candidates) and classifying the waveforms around these times on the basis of cluster formation in an  $n$ -dimensional feature space (Schmidt, 1984; Stashuk and Qu, 1996a; Lewicki, 1998). This feature space usually contains shape-related prop-

erties of the MUAP, either the candidate waveform itself or a reduced property set that captures the essential differences in shape among the different waveforms. The latter may include simple shape-based features (e.g. peak-to-peak amplitude, rise time), other time domain features (e.g. principal components (Stitt et al., 1998)), or time–frequency components (e.g. wavelet coefficients (Zouridakis and Tam, 1997; Letelier and Weber, 2000)).

Ideally, candidate MUAPs form non-overlapping clusters in this  $n$ -dimensional space. However, moment-to-moment variation in MUAP shape and superposition of multiple MUAPs cause clusters to overlap. As more motor units are recruited and their firing rates increase during increasing levels of muscle contraction, discrimination of individual MUAP signatures becomes increasingly difficult. Improvements in MUAP discrimination have been achieved by increasing the signal-to-noise ratio (e.g. spike triggered averaging (Thomas et

\* Corresponding author. Tel.: +1-518-486-2559; fax: +1-518-486-4910.

E-mail address: [schalk@wadsworth.org](mailto:schalk@wadsworth.org) (G. Schalk).

al., 1990), non-linear filtering (Fiore et al., 1996) or multichannel electrodes (Ekstedt et al., 1969)) or by optimizing existing information (e.g. by using decomposition to resolve superpositions of individual motor units into its constituent components (Mambrito and De Luca, 1984; McGill et al., 1985; Stashuk and De Luca, 1989; Joynt et al., 1991; Loudon et al., 1992; Etawil and Stashuk, 1996; Fang et al., 1999; Gut and Moschytz, 2000; Stashuk, 2001)).

Methods of MUAP discrimination based on the temporal relationships among motor unit firings have not been developed as extensively as shape-based methods. The temporal pattern of motor unit firing provides little additional information when the activity pattern is unpredictable or not controlled. Under conditions where motor units detected by shape-based methods fire at predictable intervals, addition of temporal information has been used to improve discrimination of MUAP candidates (Joynt et al., 1991; Stashuk and Qu, 1996a) and to analyze MUAP occurrence patterns using a joint interval histogram (Siebler et al., 1992). However, both approaches are based on measurements of individual inter-spike intervals (ISIs). While robust algorithms can estimate motor unit firing-pattern statistics in the presence of incorrect ISI measurements (e.g. Stashuk and Qu, 1996b), they are bound to fail when an EMG signal containing two temporally distinct spike trains whose MUAPs have shapes that are too similar to distinguish.

Alternatively, use of temporal information that does not rely on classification of individual MUAPs could be a useful addition to motor unit discrimination schemes. For example, analysis of the overall motor unit firing patterns by Fourier transform (Lange and Hartline, 1979) or autocorrelation techniques (Liu, 1989) are less dependent on individual MUAP measurements than shape-based methods. However, these global methods are strongly influenced by the shape of the individual MUAPs and the degree of superposition, limiting their applicability to classification of individual motor units.

Development of global methods for analysis of motor unit firing behavior that do not rely on MUAP shape could supplement the more commonly used shape-based methods in situations in which there is a reasonable expectation of stable firing, i.e. ISIs exhibit a stationary mean and low coefficient of variation (COV). This report describes one such approach to improving MUAP discrimination that we are developing for use in our studies of operant conditioning of the triceps surae H-reflex (see Wolpaw, 1997 for review). In developing methods for identifying single motor units in the EMG prior to the H-reflex and analyzing their firing behavior, we discovered that shape-based methods of MUAP discrimination were of limited utility. Since several thousand H-reflexes are recorded every day from behaving animals, manual definition of MUAP discrimi-

nation parameters is impractical. In addition, individual H-reflex trials can be far apart in time, making it impossible simply to infer these parameters from preceding trials. Furthermore, the necessity of using low impedance chronically implanted electrodes to record whole-muscle EMG often results in MUAP shapes that are difficult to discriminate.

The conditioning paradigm requires that the background rectified EMG remains within a defined range for 2.3–2.7 s before H-reflex elicitation. Thus, the number and firing rates of motor units that comprise this background EMG are likely to be relatively stable. Our approach to MUAP discrimination is based on the concept that underlies the Hough transform (Hough, 1959, 1962). Widely used in the field of image processing (Gonzalez and Woods, 1992), its original application was the detection of straight lines in pixel images. It transforms the pixel image in a Cartesian coordinate system into a feature space with axes that represent parameters derived from a model that describes straight lines (e.g. the distance from an origin and the angle of the line's normal vector to the  $x$ -axis). Lines in the pixel image result in clusters in the feature space and the location of the clusters correspond to the model parameters of these lines. The Hough transform is able to perform correct global classification (i.e. identification of a straight line) despite noisy local measurements (i.e. obscured pixels). In a similar fashion, we model rhythmic repetitive spike trains with two parameters and employ a modified Hough transform (MHT) of MUAP candidate occurrence times into a two-dimensional (2-D) space. MUAP spike trains with stable repetitive occurrence patterns form clusters in this space that indicate their mean rate and variability.

## 2. Methods

### 2.1. Application of the MHT to simulated single-unit spike trains

In order to identify a spike train that occurs in a stable, repetitive fashion, we envision a temporal grid with a spacing and alignment that coincides with the actual firing times of the motor unit. Temporal variation in firing times causes misalignment of the grid to the spike train. The  $i$ th time predicted by such a global grid, i.e. the expected firing time of the  $i$ th discharge of such a spike train with a given spacing (i.e. mean ISI) and alignment (i.e. a positive offset relative to an arbitrary reference time) can be described as:

$$t_i(\text{ISI}, \text{offset}) = \text{ISI}_{\text{mean}} * i + \text{offset} \quad (1)$$

As illustrated in Fig. 1(A), any expected firing occurring at time  $t_i$  is determined by both  $\text{ISI}_{\text{mean}}$  and offset. Thus, there are many possible combinations of these

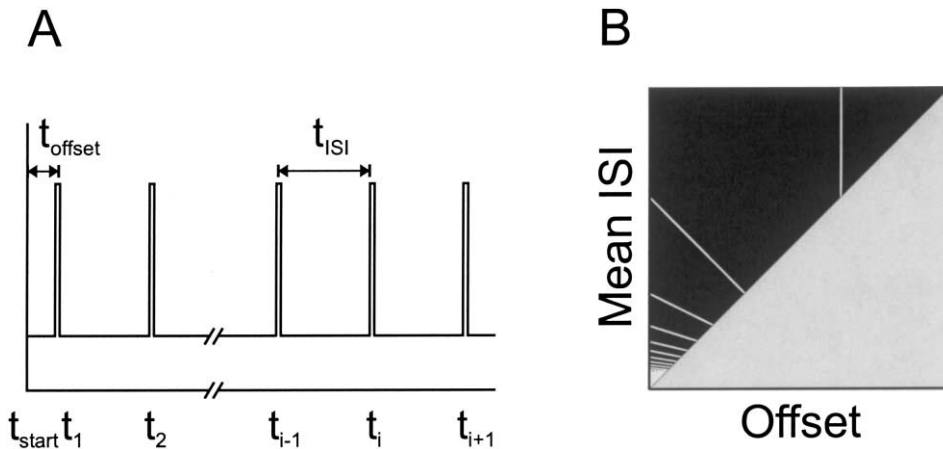


Fig. 1. (A) Model of a spike train with a constant ISI of  $t_{ISI}$  and an offset of its first spike of  $t_{offset}$  relative to an arbitrary starting time of  $t_{start}$ . (B) Resulting MHT of one arbitrary firing time  $t_i$ . The bright pattern in the feature space represents all combinations of  $t_{ISI}$  and  $t_{offset}$  describing all spike trains that would contain a spike at time  $t_i$ . The triangular region shown in gray is not part of the feature space (per definition,  $t_{offset}$  must be smaller than  $t_{ISI}$ ).

two variables (i.e. many possible spike trains) that could produce a spike at  $t_i$ . Consequently, for a given firing time  $t_i$  and an assumed  $ISI_{mean}$ , the corresponding value of offset can be calculated by iteratively subtracting  $ISI_{mean}$  from  $t_i$  to obtain the smallest non-negative remainder less than  $ISI_{mean}$ . Fig. 1(B) illustrates many of the combinations of  $ISI_{mean}$  and offset that could account for the spike firing at  $t_i$ . This mapping of a single spike in the time domain to a pattern in the ISI–offset feature space forms the basis of the MHT.

Practical implementation of the MHT required quantizing the feature space into finite intervals. This granularity defines the resolution of the feature space and thus the smallest unit of ISI that can be distinguished. In addition, the range of ISIs evaluated has to be limited (for real motor unit data, physiological properties constrain the range of values to be assessed). The MHT is implemented according to the following algorithm.

```

for each  $t_i$  do
  for each  $ISI_{mean}$  (in the feature space) do
    determine offset
    increase cell value at ( $ISI_{mean}$ , offset) by one
  repeat inner loop for all mean ISIs
repeat outer loop for all MUAP candidates
  
```

The computational complexity of the MHT is, therefore, proportional to the number of different mean ISIs in the feature space ( $n_{ISI}$ ) times the number of transformed firing times.

Each spike increments the discrete accumulator cells at the calculated ISI–offset locations (white pattern in black feature space of Fig. 1(B)). This pattern represents all possible spike trains with a firing at time  $t_i$ .

Cell values depend on the number of expected firings in the observed time period (i.e. a spike train with a constant ISI of 10 ms will have a maximum cell count

of 100 in any 1 s period, whereas a spike train with an ISI of 100 ms will have a maximum cell count of 10). To account for this uneven representation, the feature space is normalized after the MHT by dividing the accumulated value in each cell ( $cell(ISI_{mean}, offset)$ ) by the total number of discharges expected for its ISI during the analyzed time period ( $n_{exp}(ISI)$ ).

$$cell(ISI, offset) = \frac{cell(ISI_{mean}, offset)}{n_{exp}(ISI)} \quad (2)$$

Since this normalization procedure is performed on each cell in the feature space, its computational complexity is proportional to  $n_{ISI}^2$ .

## 2.2. Properties of the feature space

### 2.2.1. Feature space representation of spike trains

Repeating the MHT for all spike firing times populates the feature space with a pattern of accumulated ISI–offset combinations that describe the firing behavior of the underlying spike trains. Fig. 2 illustrates the differences in feature space patterns for spike trains that fire repetitively with constant ISIs (rows A and B) or with randomly distributed ISIs (rows C and D). For stable repetitive firing, sequential addition of spikes (increasing from column one to three) sharpens the contrast between combinations of ISI and offset that represent the actual firing rate and timing offset of the spike train. It suppresses other combinations that are randomly distributed throughout the remainder of the feature space. In contrast, randomly firing spike trains produce no focus for any one combination of ISI and offset. Sequential addition of these spikes adds a random distribution of combinations of ISI and offset that eventually fills the feature space uniformly. This transformation clearly distinguishes stable from random

firing patterns when a sufficient number of spikes are considered (e.g. compare Fig. 2(B<sub>3</sub>) with 2(D<sub>3</sub>)).

### 2.2.2. Ghosts

In addition to accumulating cell counts at the ISI–offset combination representing the actual firing rate and timing offset of a spike train with stable ISIs, the feature space also accumulates counts at other locations (Fig. 3). We refer to the bright areas corresponding to these additional locations as ghosts. They arise from the multiple ways the observed firing pattern could be generated.

For example, using a spike train with a constant ISI =  $t_{\text{ISI}}$  and offset =  $t_{\text{offset}}$ , the MHT produces an increased cell value at the expected ISI–offset combination. In addition, there is an increased cell count at

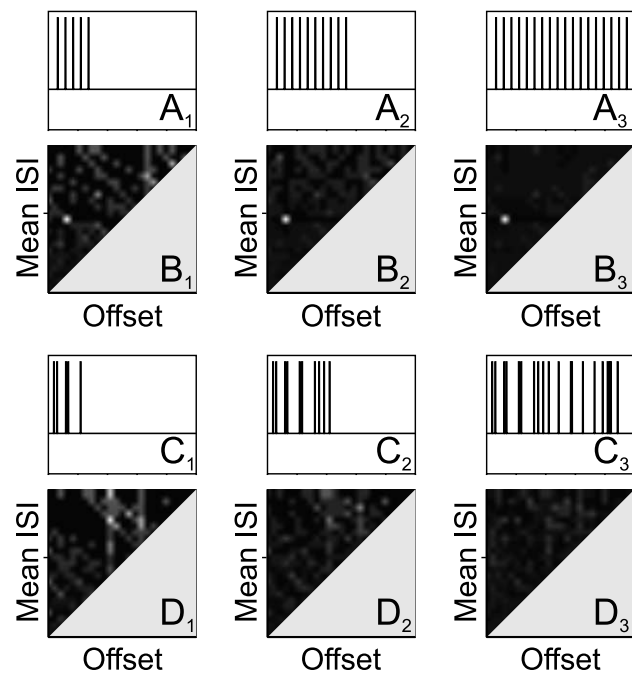


Fig. 2. Simulated spike trains with the same mean ISI having either a constant (row A) or randomly distributed (row C) ISI and their MHT feature spaces (rows B and D, respectively). The ticks on the ISI axes of the feature spaces correspond to the actual mean ISI of the simulated spike trains. Grayscale shading indicates the number of ISI–offset combinations accumulated in a given cell normalized for the expected number of spikes for its ISI (see text for description of normalization procedure). To facilitate comparison, the grayscale values of each feature space in row B were normalized to their highest value; the grayscale values of the feature spaces in row D were normalized to the same maximum value as used for the corresponding feature space in row B with the same number of spikes. Increasing the number of firings (five, ten, and 20 firings in columns 1, 2, and 3, respectively) sharpens the contrast between the underlying ISI–offset combination of the spike train with a constant ISI and the surrounding cells (row B). It decreases the contrast throughout the feature space of the spike train with a random ISI.

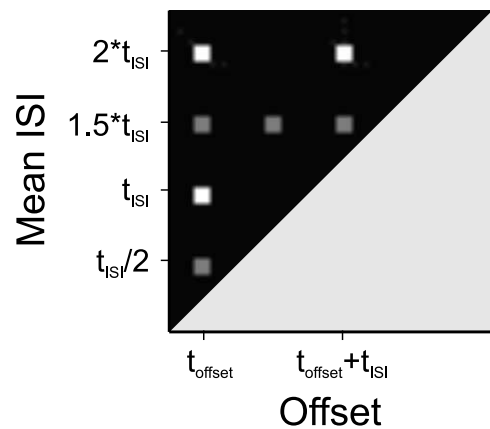


Fig. 3. MHT of a simulated spike train with a constant ISI =  $t_{\text{ISI}}$  and offset =  $t_{\text{offset}}$  produces an increased cell value at this ISI–offset combination. Increased cell values at other locations in the feature space (i.e. ghosts) reflect firing patterns that provide alternative explanations of the actual spike train (see text for further description).

ISI =  $t_{\text{ISI}}/2$  and offset =  $t_{\text{offset}}$ . This represents an alternate possible explanation of the data, a train of spikes firing at twice the rate of the actual spike train. It appears only half as bright, because the actual train contributes only every other spike of the expected number of firings for the ghost's ISI. Additional ghosts will appear at ISIs with higher integer divisors of  $t_{\text{ISI}}$  (e.g. ISI =  $t_{\text{ISI}}/3$ ,  $t_{\text{ISI}}/4$ , etc.), which are not shown for the sake of clarity. Ghosts also appear in the feature space reflecting multiples of the actual ISI. For example, the increased cell counts at ISI =  $2 \times t_{\text{ISI}}$  represent two different spike trains, each firing at half the actual rate and offset by half their mean ISI. The ghosts' cell counts are the same as that associated with the actual spike train, because the actual spike train contributes half of its firings to each of the two ghosts' cells, which produces the expected number of firings for the ghosts' ISI. It is, therefore, equally probable (without any other knowledge) that the observed spike train has been generated by the actual spike train or by two spike trains firing at half the rate of the actual train. ISIs equal to higher integer multiples of  $t_{\text{ISI}}$  will follow a similar pattern. Ghosts will also appear at non-integer multiples of the actual ISI. This is illustrated by the increased cell counts at ISI =  $1.5 \times t_{\text{ISI}}$  at three values of offset representing spike trains firing with two-thirds of the actual rate. These ghosts appear only half as bright as the cell associated with the actual ISI–offset combination, because the spike train contributes only half of the expected firings for these ghosts' ISI. Higher non-integer multiples of the ISI will produce similar patterns with increasing numbers of ghosts represented at half of the intensity of the actual ISI–offset combination.

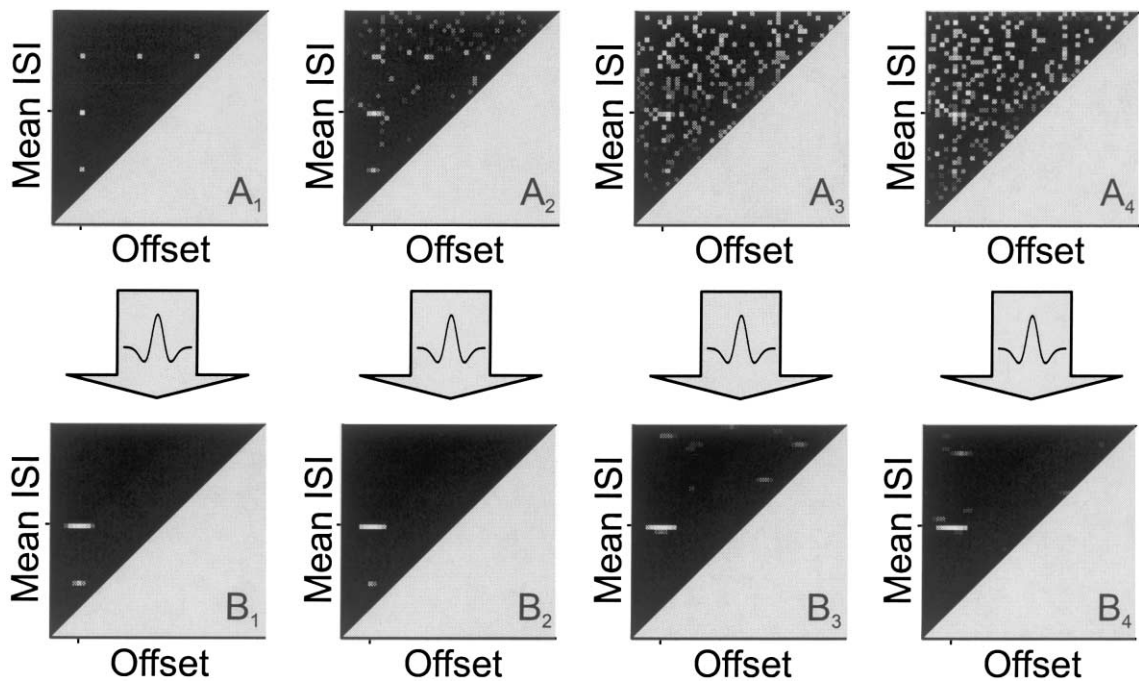


Fig. 4. Feature spaces showing the MHT of simulated spike trains before (row A) and after (row B) convolution with the  $\nabla^2G$  function. Spike trains have a mean ISI of  $t_{\text{ISI}}$  and an offset of  $t_{\text{offset}}$  (indicated by ticks on their respective axes) and a COV of the ISI of 0 ( $A_1$  and  $B_1$ ), 0.05 ( $A_2$  and  $B_2$ ), 0.10 ( $A_3$  and  $B_3$ ), and 0.15 ( $A_4$  and  $B_4$ ). Without filtering, the distinct pattern seen with COV = 0 disperses throughout the feature space with increasing ISI COV. Filtering the feature space blurs the bright spots along the offset axis (e.g. compare feature spaces at ISI =  $t_{\text{ISI}}$  in  $A_1$  and  $B_1$ ), but makes the MHT less sensitive to increasing ISI variability (e.g. compare feature spaces at ISI =  $t_{\text{ISI}}$  in  $B_1$  with those in  $B_2$ ,  $B_3$ , and  $B_4$ ). To facilitate comparisons among signal-to-noise ratios, the grayscale values were normalized to the highest value in each feature space.

### 2.3. Post-transformation processing

The model that underlies the MHT describes the predicted times of occurrence of a MUAP in a spike train given the train's mean ISI and offset. However, the ISIs of real motor units vary among sequential firings. Depending on the granularity of the feature space and ISI stability, repetitively firing motor units might contribute to cells in the feature space near the one representing the ISI–offset combination that reflects the actual average firing rate and timing offset. During repetitive firing of motor units with a stationary mean ISI, the distribution of ISIs is approximated by a normal distribution (Clamann, 1969). The ISI variability is described by its COV (i.e. the ratio of the ISI standard deviation (S.D.) to its mean ISI). COV typically falls between 0.11 and 0.14 for human motor units (Dorfman et al., 1989), but may be lower in rat soleus motor units under certain experimental conditions (e.g. see Section 4). Addition of this variability to spike trains (as defined in Eq. (1)) results in normally distributed cell counts around the location representing the average ISI–offset combination along the offset axis. This effect is evident in the MHTs of a simulated spike train firing with a constant ISI shown in Fig. 4( $A_1$ )–4( $A_4$ ). A single cell (and its ghosts) illuminates the feature space in the absence of variability (Fig.

4( $A_1$ ) for ISI COV = 0). Increasing the ISI variability broadens the distribution of illuminated cells around the expected ISI–offset locus (and ghost loci; Fig. 4( $A_2$ ) for ISI COV = 0.05). Further increases in ISI variability populate the feature space such that visual discrimination of the expected ISI–offset locus is difficult (Fig. 4( $A_3$ ) and 4( $A_4$ ) for ISI COV = 0.10 and 0.15, respectively).

We addressed this issue of ISI variability by incorporating a post-processing blurring of the feature space. After the normalization procedure, we convolved each cell value with a one-dimensional (1-D) function parallel to the offset axis. This function was the second derivative of a Gaussian distribution<sup>1</sup> ( $\nabla^2G$ , Eq. (3), Gonzalez and Woods, 1992) with amplitude normalized such that  $\nabla^2G(0, \sigma) = 1$ . We applied this function in an attempt to invert the process that led to the observed normal distribution of MUAP ISIs (Hjorth, 1991).

$$\nabla^2G(x, \sigma) = \left(1 - \frac{x^2}{\sigma^2}\right) e^{-x^2/2\sigma^2} \quad (3)$$

For each mean ISI in the feature space, we chose  $\sigma$  to roughly match the expected variation of the motor unit (for Fig. 4,  $\sigma(\text{ISI}) = 0.15 \times \text{ISI}$ ). The application of the

<sup>1</sup> Also called the Laplacian of Gaussian (LoG) or the ‘Mexican hat’ function in image processing applications.

$\nabla^2 G$  function with changing  $\sigma$ 's does not bias the results for cells at different ISI levels, because  $\int_{-\infty}^{+\infty} \nabla^2 G(x, \sigma) dx = 0$ , regardless of the value of  $\sigma$ . Fig. 4(B<sub>1</sub>)–4(B<sub>4</sub>) show the effect of this filter on the feature spaces for a stably firing unit for different degrees of ISI variability. Blurring is evident around the expected ISI–offset loci for different degrees of ISI variability (ISI COV = 0, 0.05, 0.10, and 0.15 in Fig. 4(B<sub>1</sub>), 4(B<sub>2</sub>), 4(B<sub>3</sub>), and 4(B<sub>4</sub>) respectively).

Finally, the convolution procedure is performed on each cell in the feature space and the size of the convolution window depends on  $\sigma$  (which depends on ISI). Thus, the computational complexity of this smoothing procedure is proportional to  $n_{\text{ISI}}^3$ .

### 2.3.1. Determining firing hypotheses

Spike trains with stable ISIs generate local maxima in the feature space (similar to cluster formation of shape-based features). The center-of-gravity of areas that exceed a specified threshold provide hypotheses about the ISIs and offsets of the underlying spike trains, which can be used as concurrent temporal information in subsequent analyses.

## 3. Application of the MHT to simulated multi-unit EMG data

Application of the MHT and a simple shape-based method to discrimination of simulated multi-unit EMG reveals the essential differences between them and the benefit of combining these approaches. For the purpose of these analyses, we simulated multi-unit activity by superimposing two to three different 1 s long artificial trains of repetitive MUAP occurrences having different mean ISIs, COVs of ISI, and offsets. The different MUAP waveforms used as templates were 8 ms long segments from averages of 10–20 individual MUAPs recorded at a 4 kHz sampling rate from soleus muscle of chronically implanted rats as described in Chen and Wolpaw (1995).

After synthesizing the multi-unit activity, MUAP candidates were identified with a simple algorithm. First, the algorithm identified peaks in the EMG segments that exceeded an empirically determined threshold value (which was set so as to identify even the smallest artificial MUAP). For each peak, a subsequent procedure removed all but the peak with the highest amplitude in a 4 ms window around it. The times of occurrence of the remaining peaks defined the MUAP candidates.

For our shape-based MUAP classification (i.e. assignment) method, we used a simple template-matching scheme that calculates a shape-based score for any given time in the trial (i.e. shapesscore). This score describes how closely the MUAP candidate waveform

can be described by the known MUAP template. This measure is similar to a normalized Euclidean distance measure (e.g. Stitt et al., 1998) and defined by:

$$\text{shapesscore} = 1 - \frac{\sigma^2(\text{error})}{\sigma^2(\text{signal})} \quad (4)$$

$$\text{shapesscore} = 1 - \frac{\sum_{i=1}^n (x_i - e_i)^2 - (\sum_{i=1}^n x_i - e_i)^2/n}{\sum_{i=1}^n x_i^2 - (\sum_{i=1}^n x_i)^2/n} \quad (5)$$

where  $n$  defines the number of samples in a template (i.e. 32, in this case) and  $e$  and  $x$  define the waveform of the template and the observed signal, respectively. Shapesscore is 1, if the observed signal exactly matches the template and 0, if the variance of the error (i.e. the difference between the observed signal and the template) equals the variance of the signal.

### 3.1. Feature stability

The temporal and shape-based features described above exhibit different susceptibilities to variations in MUAP shape and firing pattern. This is illustrated in Fig. 5, which shows the results of analyses of simulated multi-unit data by the template shape-based method described above (A) and the MHT method (B). The data consisted of a 1 s long target spike train consisting of 27 MUAP discharges with a mean ISI of 37.5 ms and with a COV of ISIs of 0.07. To this target spike train was added five times as many randomly distributed occurrences using a different MUAP template. Different degrees of contamination of the target spike train by the additional motor unit were simulated by varying the peak-to-peak amplitude from 0 to 100% of the amplitude of the repetitively firing unit (plotted on the axes labeled 'Amplitude Noise').

The sensitivity of the two approaches to different temporal structures was assessed by varying the serial dependence of the target spike train ISI. We created ISIs from a serially dependent model (see Eq. (6)) and from a serially independent model (see Eq. (7)).

$$t_i = \text{ISI}_{\text{mean}} * i + w_i + \text{offset} \quad (6)$$

$$t_i = t_{i-1} + \text{ISI}_{\text{mean}} + w_i \quad (7)$$

In these equations,  $t_i$  and  $t_{i-1}$  are adjacent times of discharge,  $\text{ISI}_{\text{mean}}$  is the average ISI,  $w_i$  is a Gaussian variable scaled to produce the required COV, and offset is the temporal offset of the first discharge (for Eq. (7),  $t_0 = \text{offset}$ ).

We then linearly interpolated between ISIs derived from these two models (e.g. ISIs with a serial dependence of 60% represent the sum of 0.6 times each interval produced by the serially dependent model and 0.4 times the comparable interval produced by the serially independent model).

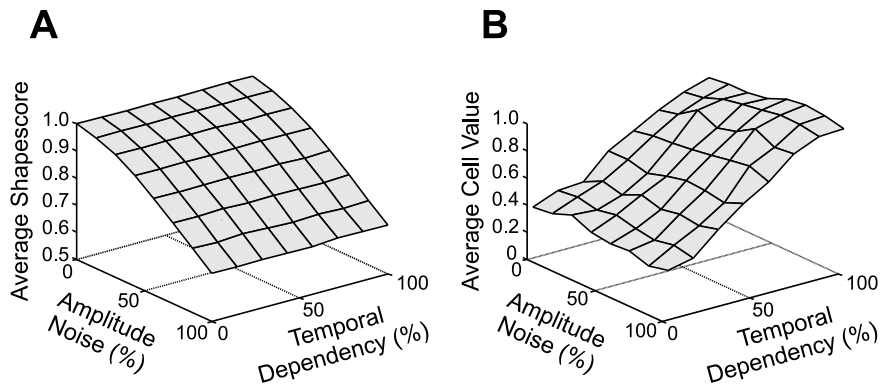


Fig. 5. Comparison of application of a shape-based classification scheme (left) and of the MHT (right) to simulated trains formed from a target MUAP shape and from a contaminating MUAP shape (see text for details of MUAP trains and definition of other parameters). Increasing the magnitude of the contaminating MUAPs (i.e. increased value on Amplitude Noise axis) deteriorated the shape-based feature provided by shapescore, but did not affect the performance of the MHT (i.e. no change in average cell value at the expected ISI–offset combination). Reducing the serial dependence of sequential ISIs (i.e. decreased value on Temporal Dependency axis) degraded performance of the MHT, but not that of the shape-based approach.

Serial dependence (plotted on the axes labeled ‘Temporal Dependency’) varied from 0% (i.e. sequential ISIs are independent of all other ISIs in the train (i.e. generated by a renewal process)) to 100% (i.e. sequential ISIs vary around the mean ISI such that larger ISIs tend to follow shorter ISIs and vice versa)<sup>2</sup>.

For each combination of Amplitude Noise and Temporal Dependency, we created 200 1 s trials. For each trial, we calculated the average shapescore at the positions of the repetitively firing unit and the cell count in the feature space at the expected location (i.e. mean ISI, mean offset) in the filtered feature space (using  $\nabla^2G$  with  $\sigma(\text{ISI}) = 0.10 \times \text{ISI}$ ). We then averaged, for each combination of Amplitude Noise and Temporal Dependency, the shapescore values (Fig. 5(A)) and the cell count values (Fig. 5(B)) and normalized the averaged cell count values to the highest value.

Fig. 5(A) shows that the average shapescore values determined by the shape-based method deteriorate with increased noise, but were not affected by the temporal alignment of the individual MUAPs. In contrast, Fig. 5(B) shows that the average cell values did not depend on the amplitude of the introduced noise, but were highly dependent on the temporal relationship of sequential occurrences. This demonstrates that decreasing serial dependence reduces the applicability of the concept of a global grid.

<sup>2</sup> Using trials with different degrees of serial dependence, we numerically evaluated the relationship between our measure and the serial correlation coefficient  $r$  calculated between adjacent intervals. Our scale of serial dependence from 0 to 100% corresponded to  $r$  values from 0 to  $-0.5$ , respectively.

### 3.2. Improved MUAP assignment by addition of temporal information

To demonstrate the potential benefit of the temporal information derived from this method, we compared the performance of the simple shape-based assignment method described above with and without application of temporal information calculated from the hypotheses generated by the MHT. In a similar fashion to before, we created 550 trials of simulated multi-unit EMG. Each trial contained three superimposed spike trains, each using a different motor unit template. The mean ISIs were 22.5, 30, and 35 ms with a COV for each ISI of 5%. ISIs exhibited serial dependence (i.e. the temporal dependency = 100%, as described in the previous section). Fig. 6 shows one of these trials.

We then calculated, for each trial and each of the three templates, the shapescore value at every time point in the trial. The upper panels in Fig. 7 illustrate the time course of shapescore of each template for the trial shown in Fig. 6 and the actual firing times of the motor unit (as expected, the shapescore values peak at the actual firing times).

For each trial, we applied the MHT to each MUAP candidate (see example in Fig. 8). The feature spaces were filtered by application of the  $\nabla^2G$  operator with  $\sigma(\text{ISI}) = 0.10 \times \text{ISI}$ . The center-of-gravity of the areas in the feature space that exceeded an empirically-determined threshold (which had the same value (i.e. 0.40) in each trial) provided firing hypotheses (i.e. ISI–offset combinations potentially representing motor units).

A simple algorithm then determined, for each template, out of all firing hypotheses the one that most

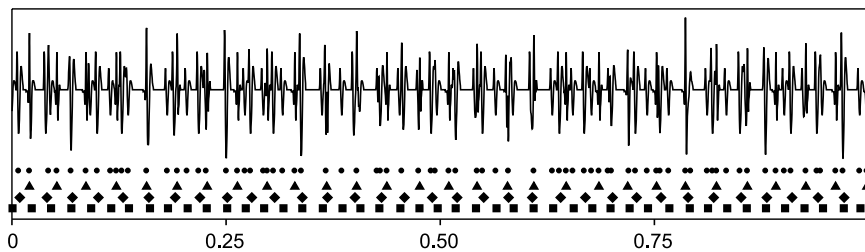


Fig. 6. Example of simulated 1 s epoch of multiunit activity formed by combining trains of three differently shaped MUAPs (recorded from rat soleus muscle) with different ISI distributions (mean ISIs = 22.5, 30.0, and 35.0 ms, COV = 0.05 for all) and offsets (2.5, 10, and 17.5 ms, respectively). Circles indicate detected motor unit candidates that were subsequently subjected to the MHT. Squares, diamonds and triangles indicate actual firing times for template I, II and III, respectively (see Fig. 7). Due to superposition, the number of motor unit candidates was approximately 20% smaller than the total number of motor unit firings in this trial.

likely produced that template's spike train<sup>3</sup>. Using its mean ISI and offset, we calculated the times  $t_i$  at which we would expect that unit to have fired. Subsequently, using these expected firing times  $t_i$ , we calculated a weighting function for each time  $t$  in the trial that represented the probability that a firing at that time would have come from the normal distributions around the expected firing times created by ISI variability (illustrated in Fig. 7):

$$\text{weight}(t) = \sum_{i=1}^n e^{-(|t-t_i|/0.25 \times \text{ISI})^2/2} \quad (8)$$

$n$  defines the number of expected MUAP occurrences in the trial,  $t$  represents any time point in the trial, and  $t_i$  stands for the expected firing times derived by the firing hypothesis.

In order to use this concurrent temporal information, we then multiplied these weighting functions with their respective shapescore time courses. We compared assignment performance with and without using the temporal information.

For each trial, we detected each of the three templates as follows: if their shapescore value (or shapescore multiplied by the weighting function) crossed a given threshold, we then identified the maximum shapescore value in a window,  $\pm 2$  ms around this point and continued to search 2 ms after this point. We then varied the assignment threshold criterion from 0 to 1. In addition, we calculated the number of correctly identified motor unit occurrences (i.e. a detected occurrence within  $\pm 0.25$  ms of an actual firing of the respective template) and the number of false positives (i.e. a detected firing not within  $\pm 0.5$  ms of an actual firing of the respective template). The results in Fig. 9 indicate that, when using

<sup>3</sup> For each ISI–offset hypothesis (and the specific template), we first calculated the timecourse of shapescore, multiplied by a weighting function derived from the hypothesis (see Eq. (8)). We then determined, in each period  $\pm \text{ISI}/2$  around each expected time of firing, the highest shapescore value. We then summed all of these values that exceeded an empirically determined threshold to calculate a score for this hypothesis and we used the hypothesis with the highest score as the 'best' hypothesis for this template.

temporal information, correct assignment of motor unit occurrences was little affected (Fig. 9(A)), but the number of false positives was markedly suppressed (Fig. 9(B)).

The low COV in this analysis (0.05) and high degree of temporal dependency (100%) provides a clear illustration of the feature space and the application of the MHT. In clinical studies, COVs of ISIs are usually higher and their temporal dependencies lower. However, analysis of the above simulations with a COV of 0.125 and a temporal dependency of 0% produced results comparable to those using the ideal values used for illustration. For example, when we used template 2 and a threshold value of 0, the temporal variation caused only modest deterioration in the percentage of correctly classified occurrences (i.e. 75 and 68% for shape-based detection alone and with the MHT, respectively). At the same time, addition of the MHT markedly reduced the number of false positives (i.e. 44 and 7%, respectively). This demonstrates that despite a higher COV and no temporal dependency, the MHT can still be useful.

#### 4. Application of the MHT to rat soleus muscle EMG

We have demonstrated the potential utility of the MHT on simulated multiunit EMG data. To complement these simulations, we show an example of how the MHT could be used to obtain temporal information that could be used to assist in the assignment of single motor unit action potential occurrences in whole muscle EMG without knowing MUAP templates a priori. We recorded signals (at a 4 kHz sampling rate) from the soleus muscle of chronically implanted rats (Chen and Wolpaw, 1995) and stored 1 s long epochs before H-reflex elicitation.

Fig. 10 shows one of these epochs. As with the simulated data, we first determined the MUAP candidates, i.e. the times of likely MUAP occurrences (see the times marked with the symbol 'x' in Fig. 10). We then subjected these to the MHT (Fig. 11). The center-of-gravity of the areas exceeding an empirically determined threshold provided hypotheses about the mean ISI and offset of the underlying spike train.

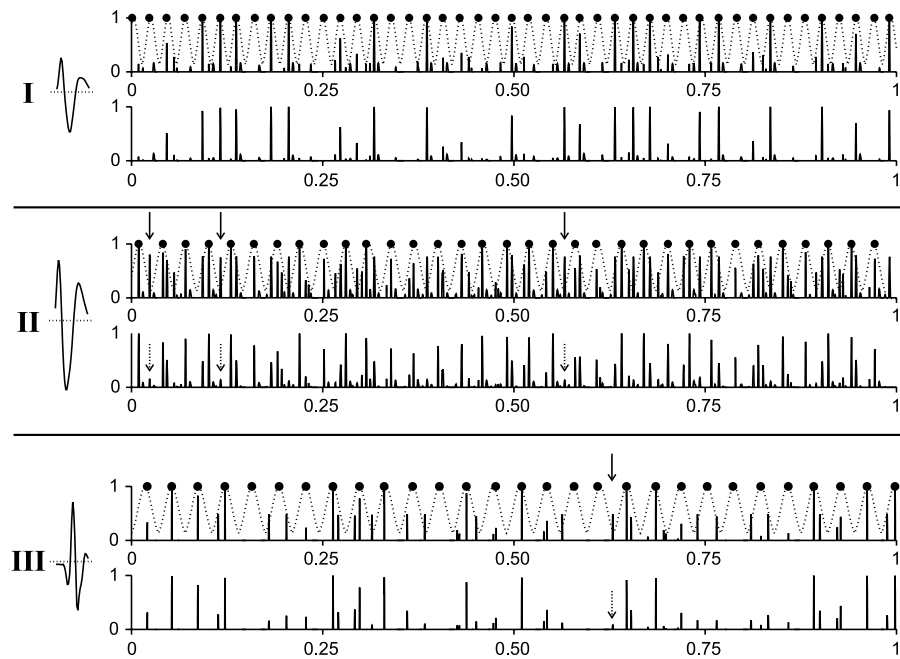


Fig. 7. Application of temporal information derived from MHT of simulated multiunit activity to shape-based MUAP discrimination. For each of the three simulated units (I, II, III), the upper panels show shapescore calculated between the simulated data and each of the MUAP templates (solid lines), the weighting functions resulting from application of the MHT (dotted lines indicating the probability that a discharge at that time was produced by the spike train predicted by the ISI–offset hypotheses ( $\sigma = 0.25 \times \text{ISI}$ )), and the actual firing times of each unit (circles). In addition to the expected peaks of shapescore at the actual firing times, occasionally there are high values of shapescore at times other than at the actual firings where the firing hypotheses predict a low probability of firing (solid arrows), indicating contamination from other MUAP shapes. Multiplication of the time courses of shapescore by the weighting functions results in a temporally enhanced correlation score (lower panels) that attenuates the contributions from the other MUAPs (dashed arrows).

Assuming that a motor unit will fire close to the firing times predicted by these hypotheses, we used this information in a shape-based classification procedure. In a similar fashion to the above, we calculated a weighting function describing the expected firing probability. Next, we eliminated all MUAP candidates for which the weighting function was smaller than a specified value (i.e. 0.65 in this example). We then removed all MUAP candidates whose polarity (i.e. the sign of the signal amplitude at the time of the MUAP candidate) differed from the polarity of the majority of the candidates. Subsequently, we calculated the peak-to-peak amplitude for each MUAP candidate and removed the 10% of the candidates whose amplitude differed most from the mean peak-to-peak amplitude. Finally, we calculated the average peak-to-peak amplitude and the COV associated with the remaining MUAP candidates. In case the COV of the peak-to-peak amplitudes was less than a empirically determined threshold (i.e. 0.25; a loose measure for whether the shapes around the MUAP candidates were sufficiently consistent), we marked the remaining motor unit candidates as belonging to one class (see circles in Fig. 10).

In the illustrated trial, the calculated mean ISI of the motor unit was 33.3 ms and its COV was 0.05. The correlation coefficient  $r$  of the occurrences was  $-0.46$ ,

which corresponds to a temporal dependency of 68%. This demonstrates that the MHT can be useful (in particular on short stretches of data), even if firings do not exhibit the ideal condition of total serial dependence (see also assessment of trials with 0% serial dependence in Section 3.2).

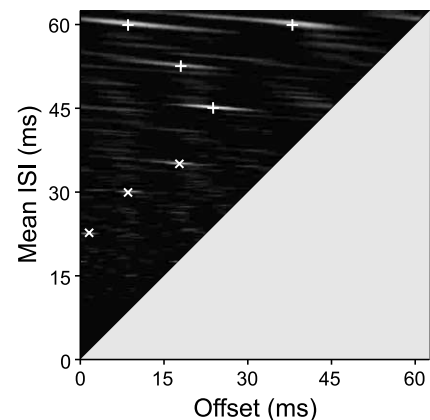


Fig. 8. Feature space (with resolution 0.25 ms) derived from the motor unit candidates shown in Fig. 6. Locations marked with the symbol 'x' identify the ISI–offset combinations of the three simulated motor units and the locations marked with the symbol '+' identify other theoretically possible firing patterns (i.e. ghosts).

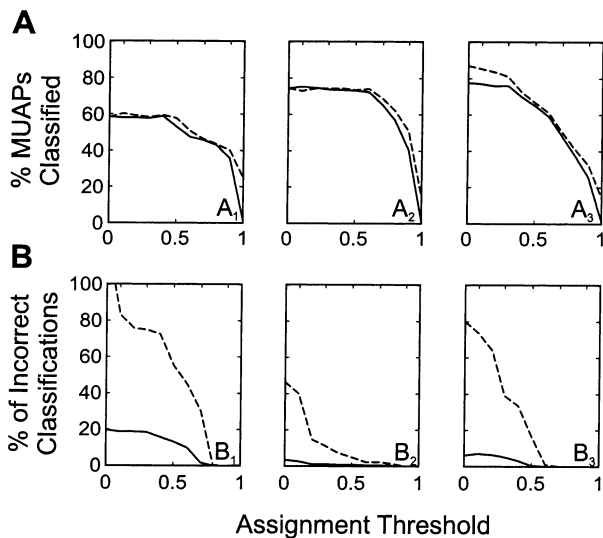


Fig. 9. Contribution of the MHT to shape-based assignment of the three MUAP templates used to simulate multiunit activity as illustrated in Fig. 7. For each template, the average percent of classified MUAPs (row A) decreases with increasing assignment threshold stringency with (solid lines) or without (dashed lines) addition of temporal information from the MHT (using the method for combining shape and temporal information illustrated in Fig. 7). The average number of incorrect classifications (i.e. false positives) expressed as a percent of the maximum possible number (row B) was markedly lower using both shape and temporal information (solid lines) than shape information alone (dashed lines), especially at low levels of assignment threshold stringency.

## 5. Discussion

### 5.1. Assumptions and limitations

The MHT readily detects spike trains with constant ISIs (see Eq. (1), and Fig. 2). However, neuronal spike trains always exhibit ISI variation. We describe the magnitude of this variation by the ISI's COV and its temporal pattern by the serial dependence of the MUAP occurrences. For any given COV, the temporal dependence is one of the main determinants of efficacy of spike train identification by the MHT. Serially dependent ISIs (e.g. long ISIs followed by short ISIs) have spike times which are multiples of the mean ISI relative to the time of the first spike. In this case, increased data segment

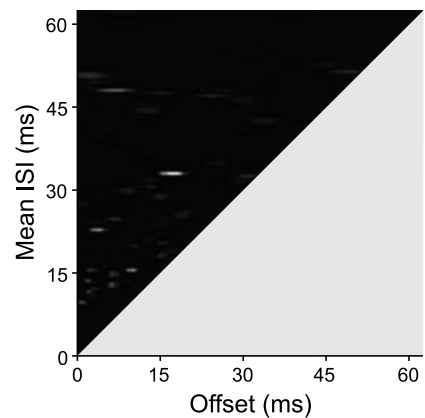


Fig. 11. Feature space calculated from the motor unit candidates shown in Fig. 10 (after post-processing with  $\sigma = 0.10 \times \text{ISI}$ , feature space resolution = 0.5 ms). The bright area centered around the intersection of mean ISI = 33 ms and offset = 16 ms identifies the firing hypothesis that describes the temporal pattern of the spike train and that subsequently assists in the identification of the actual MUAP discharges in Fig. 10.

length increases the signal-to-noise ratio in the feature space (as illustrated in Fig. 2). On the other hand, serially independent ISIs render prediction of successive spike times increasingly inaccurate as the length of time from the initial discharge increases. Thus, this independence of firing times necessarily imposes practical limitations on data segment length that can be used, in that using longer data segments to improve the signal-to-noise ratio will also cause hot spots to be increasingly blurred.

ISIs of neuronal spike trains rarely exhibit complete temporal independence (e.g. Perkel et al., 1967). In healthy humans, MUAP ISIs exhibit a modest degree of serial dependence (Andreassen and Rosenfalck, 1978; Wiegner et al., 1993; Yan et al., 1998). Our preliminary studies in chronically implanted rats indicate that MUAP ISI variation exhibits some serial dependence (see Section 4). Even at these low levels of serial dependence, the MHT can detect MUAP trains (see Fig. 11).

The performance of any classification method relies on the ability to discriminate features that are extracted from a signal. In this initial analysis, the MHT appears to be relatively unaffected by the firings of other motor units. However, many other factors (e.g. the observed

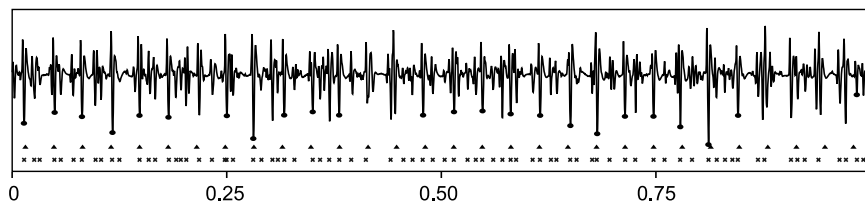


Fig. 10. Example of one 1 s epoch of whole muscle EMG recorded from soleus muscle in rats prior to H-reflex elicitation. The motor unit candidates that were subsequently subjected to the MHT are identified by the symbol 'x'. The triangles indicate the expected firing times based on the firing hypothesis derived from the MHT in Fig. 11. Circles mark the individual MUAP discharges identified using these expected firing times and a shape-based classification procedure (see text).

time frame, missed MUAP candidates due to superposition, larger number of MUAP candidates with increasing EMG levels) could influence temporal discrimination (i.e. the signal-to-noise ratio in the feature space). The extent to which these factors decrease this signal-to-noise ratio remains to be explored.

In summary, the utility of the MHT will be greatest in situations in which the COV of a spike train is low and/or the ISIs in the observed spike train exhibit some degree of serial dependence.

### 5.2. Advantages

Spike detection and identification schemes that use temporal information to augment MUAP assignment decisions have been described (e.g. Stashuk and Qu, 1996a,b). However, they all rely on measurements of individual ISIs and thus cannot aid in situations in which MUAP shapes produced by multiple motor units are too similar to be distinguished. As a result, the MHT could provide additional information that no current method can provide—an advantage that is particularly important in situations in which data is scarce.

Furthermore, even under nominally stable conditions (e.g. during the pre-stimulus background period of the H-reflex conditioning task (Chen and Wolpaw, 1995)), it is unlikely that every motor unit that contributes to the observed EMG signal will fire at a constant rate or exhibit the necessary amount of serial dependence. Thus, the MHT might only deliver information on some of the motor unit spike trains that underlie the observed EMG signal. In the worst case, the MHT would not provide any additional information, but at the same time would not impair implementation of other approaches.

The MHT is potentially beneficial in MUAP detection and classification, in part because it relies on assumptions that are different from those of classical shape-based methods, which assume MUAP shape stability. Since the MHT method employs a global rather than a local approach (i.e. detected ISI–offset combinations rather than individually classified motor unit discharges), it is difficult to compare its efficacy in MUAP discrimination directly to that of a shape-based method. Thus, we demonstrated that use of temporal information concurrent with shape information improves the ability to identify MUAPs.

Finally, conventional schemes that take advantage of temporal information require accurate MUAP identification that typically only complex multi-pass schemes may provide. The MHT is easy to implement and has little associated computational cost. Its incorporation into conventional schemes might be beneficial in situations in which the implementation of more complex or computationally costly schemes are not practical or necessary. In certain clinical applications in which only firing rate and firing variability are of importance (and not individual

discharge times), the MHT could even be used without having to implement any shape-based method.

### 5.3. Potential improvements in implementation of the MHT

We have used a simple thresholding procedure to detect firing hypotheses in the feature space. More sophisticated methods could improve detection performance by taking the number of MUAP candidates and the resolution of the feature space into account to test whether one particular bin is statistically different than adjacent bins.

To demonstrate the principle of combining information from both the MHT and the shape-based assignment method, we multiplied the simple weighting function with the time course of shapescore. More sophisticated methods might take better advantage of this additional piece of information. In addition, we used a very simple motor unit classification procedure to demonstrate the benefit of the MHT. Modern classification schemes would undoubtedly result in better performance. Nevertheless, even these algorithms would likely benefit from additional temporal information.

The Hough transform has been studied extensively in the field of image processing. While originally devised to detect straight lines in pixel images, the concept of the Hough transform is applicable to a wide variety of parametric curves (Ballard, 1981; Olson, 1999). In addition, more sophisticated algorithms optimize the information in the feature space (van Veen and Groen, 1981; Immerkær, 1998). Compared with its counterparts in image processing, the MHT is in an early stage of development. Adaptation of the more advanced implementations of the Hough transform to the MHT may extend its reach, e.g. from the detection of stable repetitive patterns to oscillating or other patterns that can be described by simple models, or might optimize the information in the feature space, e.g. by implementing variable granularity depending on the ISI.

Improved spike assignment is not the only application for this method. It could provide an estimate of the mean firing rate of motor units in recordings, in which some of the discharges have been missed (or in which false positives contaminate the estimate of firing statistics), or it might be used to separate a repetitively firing unit from false positives in a stage subsequent to shape-based classification. Firing variability could be estimated by analyzing the distribution of cell counts around a detected firing hypothesis in the feature space. In addition, the method is not restricted to 2-D. Shape-based features derived from each MUAP candidate could serve as additional dimensions in the feature space, thus opening the possibility for concurrent temporal and shape-based recognition in a single method. However, the necessity of searching the entire feature space imposes computa-

tional limits on the number of dimensions that could be used in practical applications. No matter how the MHT might be implemented, additional information will always prove beneficial and, therefore, this transformation adds an effective new avenue to pursue the difficult problem of MUAP detection and classification.

## Acknowledgements

We thank Dr Dennis J. McFarland for his valuable advice in regard to statistical analysis. We also thank Dr Xiang-Yang Chen for providing the EMG recordings from which the motor unit action potential templates were extracted and which were used to produce Figs. 10 and 11. This work was supported by the National Institutes of Health (Grant NS22189 (JRW)).

## References

- Andreassen S, Rosenfalck A. Impaired regulation of the firing pattern of single motor units. *Muscle Nerve* 1978;1(5):416–8.
- Ballard D. Generalizing the Hough transform to detect arbitrary shapes. *Pattern Recogn* 1981;13:111–22.
- Chen X, Wolpaw J. Operant conditioning of H-reflex in freely moving rats. *J Neurophysiol* 1995;73(1):411–5.
- Clamann H. Statistical analysis of motor unit firing patterns in a human skeletal muscle. *Biophys J* 1969;9(10):1233–51.
- Dorfman L, Howard J, McGill K. Motor unit firing rates and firing rate variability in the detection of neuromuscular disorders. *Electroencephalogr Clin Neurophysiol* 1989;73(3):215–24.
- Ekstedt J, Haggqvist P, Stalberg E. The construction of needle multielectrodes for single fiber electromyography. *Electroencephalogr Clin Neurophysiol* 1969;27(5):540–3.
- Etawil H, Stashuk D. Resolving superimposed motor unit action potentials. *Med Biol Eng Comput* 1996;34(1):33–40.
- Fang J, Agarwal G, Shahani B. Decomposition of multiunit electromyographic signals. *IEEE Trans Biomed Eng* 1999;46(6):685–97.
- Fiore L, Corsini G, Geppetti L. Application of non-linear filters based on the median filter to experimental and simulated multiunit neural recordings. *J Neurosci Meth* 1996;70(2):177–84.
- Gonzalez R, Woods R. *Digital Image Processing*. Addison-Wesley, 1992.
- Gut R, Moschytz G. High-precision EMG signal decomposition using communication techniques. *IEEE Trans Signal Proc* 2000;48(9):2487–94.
- Hjorth B. Principles for transformation of scalp EEG from potential field into source distribution. *J Clin Neurophysiol* 1991;8(4):391–6.
- Hough P. Machine analysis of bubble chamber pictures. *International Conference on High-Energy Accelerators and Instrumentation*, CERN, 1959.
- Hough P. *Methods and Means for Recognizing Complex Patterns*. U.S. Patent 3069654, 1962.
- Immerkær J. Some remarks on the straight line Hough transform. *Pattern Recogn Lett* 1998;19:1133–5.
- Joynt R, Erlandson R, Wu S, Wang C. Electromyography interference pattern decomposition. *Arch Phys Med Rehab* 1991;72(8):567–72.
- Lange G, Hartline P. Fourier analysis of spike train data. *Biol Cybern* 1979;34(1):31–4.
- Letelier J, Weber P. Spike sorting based on discrete wavelet transform coefficients. *J Neurosci Meth* 2000;101(2):93–106.
- Lewicki M. A review of methods for spike sorting: the detection and classification of neural action potentials. *Network-Comp Neural* 1998;9(4):R53–78.
- Liu L. A method of neuronal spike train study based on autoregressive analysis. *Biol Cybern* 1989;61(4):289–93.
- Loudon G, Jones N, Sehmi A. New signal processing techniques for the decomposition of EMG signals. *Med Biol Eng Comput* 1992;30(6):591–9.
- Mambrito B, De Luca C. A technique for the detection, decomposition and analysis of the EMG signal. *Electroencephalogr Clin Neurophysiol* 1984;58(2):175–88.
- McGill K, Cummins K, Dorfman L. Automatic decomposition of the clinical electromyogram. *IEEE Trans Biomed Eng* 1985;32(7):470–7.
- Olson C. Constrained Hough transforms for curve detection. *Comput Vis Image Und* 1999;73(3):329–45.
- Perkel D, Gerstein G, Moore G. Neuronal spike trains and stochastic point processes. I. The single spike train. *Biophys J* 1967;7(4):391–418.
- Schmidt E. Computer separation of multi-unit neuroelectric data: a review. *J Neurosci Meth* 1984;12:95–111.
- Siebler M, Köller H, Rose G, Müller H. An improved graphical method for pattern recognition from spike trains of spontaneously active neurons. *Exp Brain Res* 1992;90(1):141–6.
- Stashuk D. EMG signal decomposition: how can it be accomplished and used? *J Electromyogr Kines* 2001;11:151–73.
- Stashuk D, De Luca C. Update on the decomposition and analysis of EMG signals. In: Desmedt J, editor. *Computer-Aided Electromyography and Expert Systems*. Elsevier, 1989.
- Stashuk D, Qu Y. Adaptive motor unit action potential clustering using shape and temporal information. *Med Biol Eng Comput* 1996a;34(1):41–9.
- Stashuk D, Qu Y. Robust method for estimating motor unit firing pattern statistics. *Med Biol Eng Comput* 1996b;34(1):50–7.
- Stitt J, Gaumont R, Frazier J, Hanson F. Action potential classifiers—a functional comparison of template matching, principal components analysis and an artificial neural network. *Chem Senses* 1998;23(5):531–9.
- Thomas C, Bigland-Ritchie B, Westling G, Johansson R. A comparison of human thenar motor-unit properties studied by intraneural motor-axon stimulation and spike-triggered averaging. *J Neurophysiol* 1990;64(4):1347–51.
- van Veen T, Groen F. Discretization errors in the Hough transform. *Pattern Recogn* 1981;14:137–45.
- Wiegner A, Wierzbicka M, Davies L, Young R. Discharge properties of single motor units in patients with spinal cord injuries. *Muscle Nerve* 1993;16(6):661–71.
- Wolpaw J. The complex structure of a simple memory. *Trends Neurosci* 1997;20(12):588–94.
- Yan K, Fang J, Shahani B. Motor unit discharge behaviors in stroke patients. *Muscle Nerve* 1998;21(11):1502–6.
- Zouridakis G, Tam D. Multi-unit spike discrimination using wavelet transforms. *Comput Biol Med* 1997;27(1):9–18.